Low-power-consumption ultraviolet photodetector based on p-NiO/SiO_2/n-ZnO

Menghan Jia[1,3], Fang Wang[3], Libin Tang[2,3]*, Jinzhong Xiang[1,3]*, Kar Seng Teng[4]*, Shu Ping Lau[5], and Yanfei Lü[1]*

[1]*School of Physics and Astronomy, Yunnan University, Kunming 650500, People's Republic of China*

[2]*Kunming Institute of Physics, Kunming 650223, People's Republic of China*

[3]*Yunnan State Key Laboratory of Advanced Photoelectric Materials and Devices, Kunming 650223, People's Republic of China*

[4]*Department of Electronic and Electrical Engineering, Swansea University, Bay Campus, Fabian Way, Swansea SA1 8EN, United Kingdom*

[5]*Department of Applied Physics, The Hong Kong Polytechnic University, Hung Hom, Kowloon, Hong Kong, People's Republic of China*

E-mail: sscitang@163.com, optik@sina.com, jzhxiang@ynu.edu.cn, k.s.teng@swansea.ac.uk

Abstract: Ultraviolet (UV) photodetector has found extensive applications, ranging from optical communication to ozone sensing. Wide bandgap metal oxide heterostructures have gained significant interest in the development of UV photodetectors due to their excellent electronic and optical properties, as well as ease of fabrication. However, there are surface and interface issues at these heterostructures that have detrimental effects on device performance. In this work, UV photodetector consisting of p-NiO/SiO_2/n-ZnO heterostructure was prepared by RF magnetron sputtering method. The device exhibited remarkable performances, such as having a rectification ratio of 57, responsivity (R) of 5.77 AW^{-1}, external quantum efficiency (EQE) of 1.96×10^3 % and rise time of 0.048 s at a low power consumption of -0.1 V under 365 nm UV irradiation. This work demonstrated a method for low-cost fabrication of photodetectors with rectification behavior and at low power consumption.

Keywords: UV photodetector; Metal oxide semiconductor; Heterostructure; Low power consumption

1. Introduction

There has been much research interest in the development of ultraviolet (UV) photodetectors. These UV photodetectors have found wide-ranging applications in many exciting fields, such as optical communication, biochemical analysis, flame and ozone detections and so on [1]. To date, most UV photodetectors are based on wide bandgap metal oxide semiconductors (e.g. ZnO [2-4], NiO [5, 6], TiO_2 [7, 8], SnO_2 [9, 10] and Ga_2O_3 [11-13] etc.) due to their excellent electronic, chemical and optical properties. For example, these metal oxide-based photodetectors do not oxidize easily and exhibit sensitive photoresponse. Furthermore, they are easy to operate and can be miniaturized [14, 15]. Among the metal oxides, ZnO is a popular material for UV photodetectors since the late '90s. The initial use of ZnO microcrystal in light-pumped UV laser emission at room temperature performed by Zu [16] et al. has resulted in an upsurge in the research interest of ZnO and its optoelectronic properties. Over the years, there has been much effort in enhancing the performance of ZnO based UV photodetectors even until today.

Many groups have attempted to enhance the performance of UV photodetectors by using heterostructure consisting of two different metal oxide semiconductors. As it is difficult to prepare stable p-type ZnO, this presents a major challenge to produce reliable UV photodetectors based on p-ZnO/n-ZnO structure. Hence, this has led to the study and optimization of ZnO based UV photodetectors using heterostructure consisting of a different p-type material that matches the lattice constant of ZnO and is reasonably stable. NiO is a suitable candidate as it is a stable intrinsic p-type material, which can form a heterostructure with n-type ZnO. Recently, Kim [17] et al. prepared UV photodetector based on p-NiO/n-ZnO heterostructure on ITO substrate. The device exhibited high gain with rise and fall time of 0.2 and 0.18 s, respectively. More recently, Zhang [18] et al. fabricated UV photodetector based on ZnO/NiO nanofiber arrays by electrospinning technique. The maximum responsivity of the device was 0.415 mAW^{-1} and rise/decay time of 7.5 s/4.8 s. This can be attributed to the matching of the energy bands of NiO and ZnO. However, the rectification characteristics and response time of these devices operating at a low power consumption still need to be improved.

In this work, UV photodetector based on p-NiO/SiO_2/n-ZnO heterostructures deposited on ITO coated-quartz substrate using magnetron sputtering technique was studied. An UV photodetector based on p-NiO/i-SiO_2/n-ZnO nanowire was previously reported by others [19], which demonstrated the fastest response time with rise and decay time of 4 s and 3 s, respectively at -2 V. Herein, a photodetector was fabricated using a facile magnetron sputtering method, which was used to prepare three different films. Importantly, the device exhibited excellent response time (e.g., rise time ~ 0.048 s and decay time ~ 0.108 s + 1.66 s) at a small bias of -0.1 V. The photodetector reported in this study was improved by two orders of magnitude as compared to that based on ZnO nanowire. In addition, the photodetector prepared by us exhibited excellent sensitivity, good rectification characteristics and low dark current. It also demonstrated ultrahigh responsivity (R) of 5.77 AW^{-1} under 365 nm irradiation at 2 V. Furthermore, the maximum detectivity (D^*) was 1.51×10^{11} Jones under 365 nm illumination at a bias voltage of 2 V.

2. Materials and Methods

NiO, ZnO and SiO_2 targets (99.99%) were purchased from Zhongnuo Advanced Material (Beijing) Technology Co. Ltd. Quartz substrate was purchased from Beijing Physike Technology Co. Ltd. ITO-coated quartz substrate was purchased from Beijing Jinji Aomeng Technology Co. Ltd. All chemical reagents were used without further purification.

NiO, ZnO and SiO_2 films were prepared by RF magnetron sputtering at room temperature. Prior to deposition, the substrates were cleaned in a mixed solution of ammonia water, hydrogen peroxide and deionized water at 80 °C for 30 min. After washing and drying, NiO film was deposited at a sputtering power of 200 W and a pressure of 0.6 Pa with a flow of oxygen and argon at a ratio of 1:1. As for SiO_2 film, it was deposited using a sputtering power of 100 W at a pressure of 0.8 Pa with 1:2 flow ratio of oxygen and argon. ZnO film was deposited at a power of 75 W, a pressure of 0.6 Pa and 1:2 flow ratio of oxygen and argon. Subsequently, the deposited films were annealed in air at 300 °C at a rate of 10 °C/min for 30 min in a tubular furnace.

Crystalline structure of NiO and ZnO films were studied using transmission electron microscope (TEM, JEM-2100). Surface morphology of NiO and ZnO films were characterized using atomic force microscope (AFM, SPA-400). Absorption and diffraction spectra of the NiO film (i.e., ITO/NiO) and the structure of NiO/SiO_2/ZnO (i.e., ITO/NiO/SiO_2/ZnO) were obtained using UV-Vis spectroscopy (iHR-320) and X-ray diffraction (XRD, EMPYREAN). Cross-sectional image of the ITO/NiO/SiO_2/n-ZnO photodetector was acquired using scanning electron microscope (SEM, Hitachi S-3400N). Current-voltage (*I-V*) measurements on the photodetector were performed using a Keithley 2400 source meter. All measurements were conducted at room temperature.

3. Results and discussion

TEM characterization was performed on the as-prepared films to study its crystal structure. Fig. 1(a) and (b) show TEM and HRTEM images of the NiO film, respectively. The lattice fringe spacing of crystal plane (200), (220), $(\bar{2}00)$ and $(\bar{2}\bar{2}0)$ was 2.08, 1.48, 2.08 and 1.48 Å, respectively. This is in good agreement with previously reported work in the literature [20]. The inset of Fig. 1(b) shows the fast Fourier transform (FFT) pattern of NiO, which revealed a crystal structure belonging to cubic phase (similar to NaCl structure) and Fm3m space group as illustrated in Fig. 1(c). TEM and HRTEM images of the ZnO film are shown in Fig. 1(d) and (e), respectively. The lattice fringe spacing of crystal plane (101), (100) and (002) was 2.47, 2.79 and 2.59 Å, respectively and is consistent with previously reported work [4]. The FFT pattern of the ZnO film is shown in the inset of Fig. 1(e). It revealed a hexagonal wurtzite structure, which belonged to hexagonal phase (e.g., 6mm point group) and P63mc space group [21]. A schematic diagram of ZnO crystal structure is depicted in Fig. 1(f).

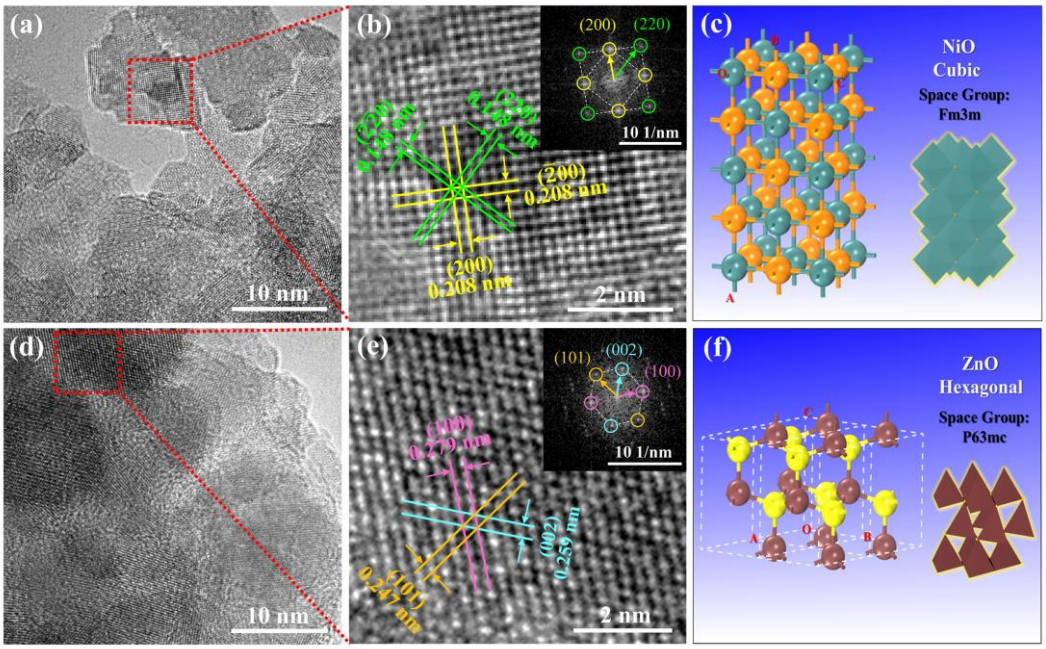

Fig. 1. (a)-(b) TEM and HRTEM (inset: FFT pattern) images of the NiO film. (c) Schematic diagram showing crystal structure of NiO. (d)-(e) TEM and HRTEM (inset: FFT pattern) images of the ZnO film. (f) Schematic diagram showing crystal structure of ZnO.

AFM topography images of the films are shown in Fig. 2(a)-(d). The AFM images of NiO and ZnO films showed uniform granular surface topography with relatively small root-mean-square (RMS) surface roughness of 1.12 and 0.61 nm as observed in Fig. 2(b) and (d), respectively. The RMS roughness of ZnO film was smaller than that of NiO film. Hence, the relatively smooth surface of ZnO film was suitable for deposition of electrodes for device characterization as it would increase the interfacial area between the ZnO film and Al electrodes [22]. This could enhance device performance as the electrodes can effectively collect the separated photogenerated carriers. UV-Vis absorption spectra of NiO and NiO/SiO_2/ZnO are shown in Fig. 2(e). Both samples exhibited strong UV absorption between 190 and 380 nm, and almost no absorption in the visible light band, thus implying they are suitable for detecting UV band. It is worth noting that the absorption edge of NiO (~ 350 nm) was slightly steeper than that of NiO/SiO_2/ZnO (~ 389 nm). The cutoff edge corresponding to the structure of NiO/SiO_2/ZnO was red shifted after the deposition of ZnO film. This is mainly due to the optical bandgap of ZnO is smaller than that of NiO, therefore resulting in a significant increase in the absorption cutoff wavelength of NiO/SiO_2/ZnO in the range of 325 to 400 nm. Fig. 2(f) shows the XRD patterns of ITO/NiO/SiO_2/ZnO, ITO/NiO and ITO-coated quartz substrate. It is important to note that the unmarked diffraction peaks in the XRD patterns of ITO/NiO/SiO_2/ZnO (purple line) and ITO/NiO (blue line) belonged to ITO-coated quartz substrate. By comparison, there were two characteristic peaks associated with NiO (111) (as shown in the inset) and (200) crystal planes of cubic phase in the ITO/NiO sample. Hexagonal ZnO (002) and (102) crystal planes were observed in the ITO/NiO/SiO_2/ZnO sample. The observed patterns are consistent with previous works reported by Zhang et al [18]. These characteristic peaks suggest

that the ZnO film has preferential orientation along the (002) crystal plane. This is in good agreement with the above TEM results.

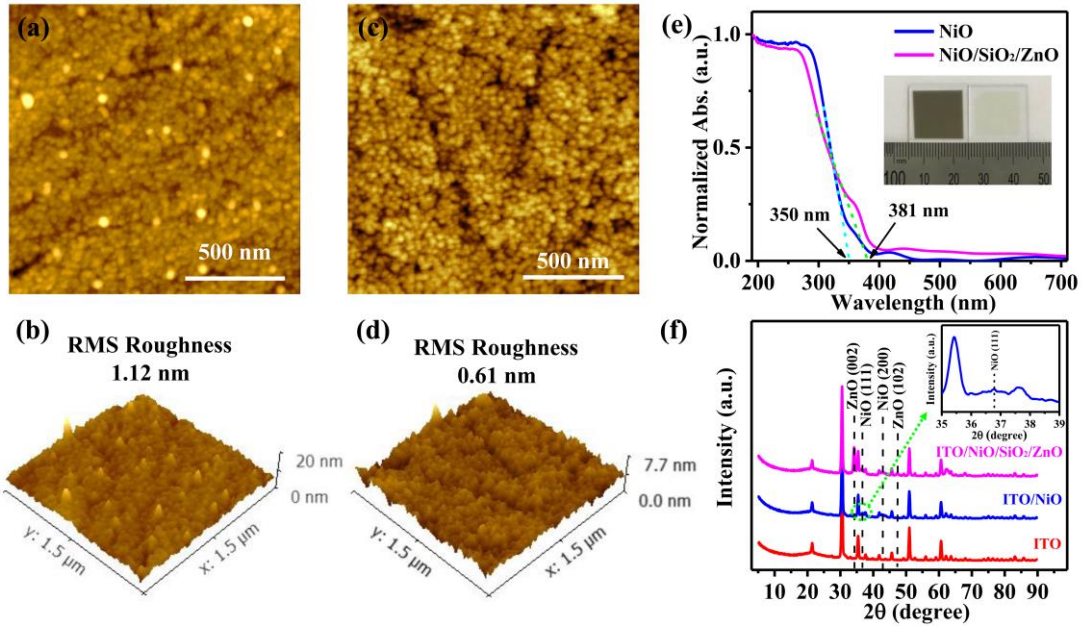

Fig. 2. AFM topography images of (a)-(b) the NiO and (c)-(d) ZnO films. (e) UV-Vis absorption spectrum of NiO and NiO/SiO_2/ZnO, and the inset shows optical images of as-grown (left) and annealed (right) NiO films on ITO-coated quartz substrate. (f) XRD patterns of ITO/NiO/SiO_2/ZnO, ITO/NiO and ITO coated quartz substrate. Inset shows a partially enlarged pattern from ITO/NiO.

A UV photodetector, consisting of NiO/SiO_2/ZnO heterostructures, was fabricated. Fig. 3(a) shows a schematic diagram illustrating the fabrication process of the photodetector. Firstly, NiO film was sputtered on an ITO coated-quartz substrate by RF magnetron sputtering. This was followed by sputtering of SiO_2 film as an insulating layer having a thickness of ~22 nm. Finally, ZnO film was sputtered on the SiO_2. Same sputtering conditions were used as described above. After deposition, the films were annealed in air at 300 ℃ for 30 min at a rate of 10 °C/min. Al electrode (2×2 mm^2) was then vapor-deposited on to the surface of ZnO film. Gold wires were attached to the ITO and Al electrodes using silver paste. Fig. 3(b) shows the vertical structure of the UV photodetector comprising of ITO/p-NiO/SiO_2/n-ZnO/Al. Cross-sectional SEM image of the photodetector is shown in Fig. 3(c). The thickness of each deposited layer can be estimated from the image. The thickness of the NiO, SiO_2 and ZnO films was estimated to be about 134, 22 and 103 nm, respectively. Fig. 3(d) illustrates an energy band diagram of the photodetector. The wide bandgap of the NiO and ZnO films is sensitive to UV light. Furthermore, the optical bandgap energy (E_g) of these films can be calculated using Eq. (A.1) [23, 24]. According to the film thickness estimated by SEM, the E_g of NiO and ZnO films can be determined from Fig. A.1(a) and (b) of the Supplementary material, which revealed a value of 3.63 and 3.23 eV, respectively. These values are very close to the theoretical bandgap of the films [2, 25, 26].

Under UV illumination (hv), valence electrons obtain enough energy to transit into the conduction band, hence generating electron-hole pairs. These photogenerated

electron-hole pairs are separated by the built-in electric field and collected by the respective electrodes. The generated carriers could tunnel through the 'potential barrier' (introduced by the SiO_2 layer) between the NiO and ZnO films. It is possible that there are some intrinsic defects in the NiO and ZnO films, which can introduce gap states in the band gap. Since these gap states are close to the band edges, some carriers from the valence band and conduction band can be captured by the gap states and these carriers will be constrained at the interface [27]. However, the SiO_2 interlayer can suppress the surface defects of the film, thus inhibiting carrier recombination at the interface and improving the transport efficiency of carriers [33]. This would limit the leakage current, therefore improving the photoelectric performance of the device.

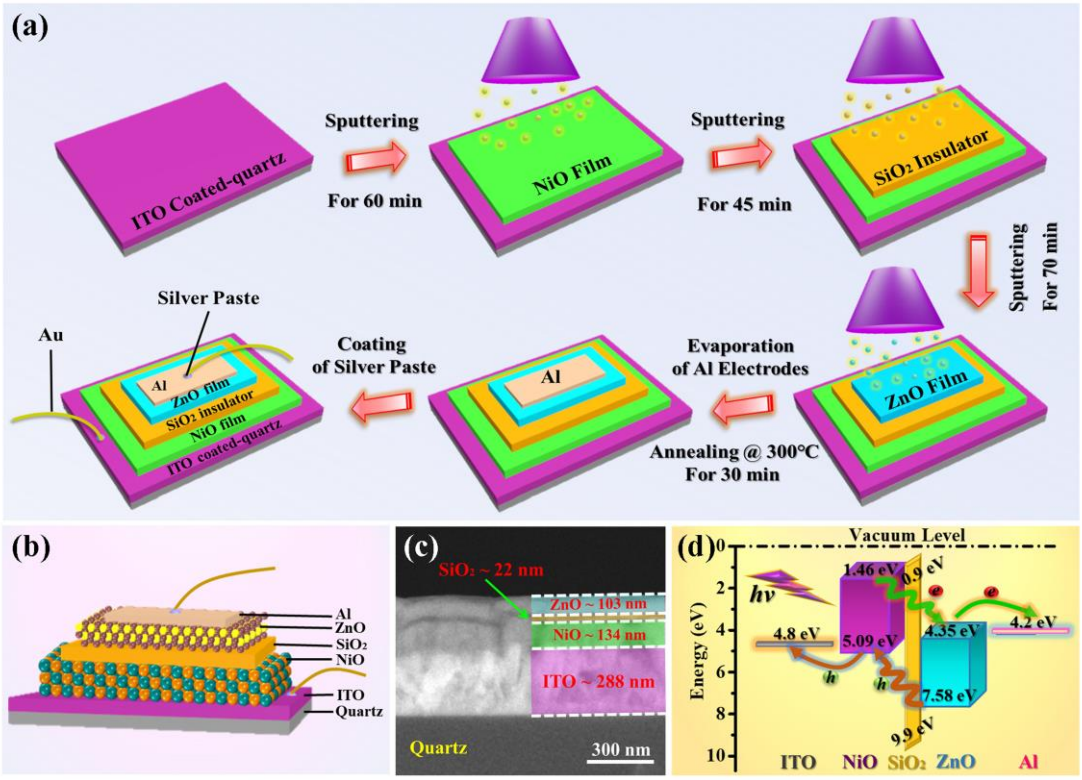

Fig. 3. (a) Schematic diagrams illustrating the fabrication process of the ITO/NiO/SiO_2/ZnO/Al photodetector. (b) Schematic diagram showing the device structure of the UV photodetector. (c) Cross-sectional SEM image of the photodetector. (d) Energy band diagram of the photodetector.

Prior to performing *I-V* measurements on the NiO/SiO_2/ZnO photodetector, the contact behavior between the Al electrode and ZnO film was examined. As shown in Fig. 4(a), the *I-V* plot acquired from the Al/ZnO/Al structure was linear, thus indicating an ohmic contact was formed between the Al electrode and ZnO film. *I-V* characteristic curves under dark and light conditions of the NiO/SiO_2/ZnO photodetector and a separate *I-V* curve of the dark condition are shown in Fig. 4(b) and (c), respectively. Measurements were performed on the backlight incident device under 365 nm UV light with photo power densities of 0.3, 1.6, 3.6 and 5.7 $mWcm^{-2}$. The rectification ratio (e.g., I_{dark}(+2 V)/I_{dark}(-2 V)) was approximately 57 without irradiation. Accordingly, the dark currents were 183.2 μA and 3.2 μA at 2 V and -2 V biases, respectively. An increase in the dark current was observed under positive bias. This demonstrated the typical

rectifying behavior and the formation of the NiO/SiO_2/ZnO heterostructures. The results showed excellent rectification characteristics and photoresponse of the photodetector. When the photodetector was exposed to 365 nm UV illumination, the photocurrent increased sharply. As shown, an increase in the photo power density has resulted in an increase in the current. Therefore, the p-NiO/SiO_2/n-ZnO photodetector can produce photogenerated carriers under UV illumination.

The effect of bias voltage on the responsivity (R) of the device is shown in Fig. 4(d). R is related to the photocurrent density (J_{ph}) according to the following equation [4, 28]:

$$R = \frac{J_{ph}}{P_{opt}} \tag{1}$$

where P_{opt} is photo power density, such as 0.3, 1.6, 3.6 and 5.7 $mWcm^{-2}$. A decrease in R was evident from Fig. 4(d) as photo power density of incident light was increased under fixed bias voltage. The maximum value of R was 5.77 AW^{-1} at bias voltage of 2 V and low photo power density of 0.3 $mWcm^{-2}$.

Detectivity (D^*), which describes the smallest detectable signals, is another important figure of merit when evaluating the performance of photodetectors. It can be calculated using the equation as follows [29]:

$$D^* = \frac{R}{\sqrt{2e|J_d|}} \tag{2}$$

where e is electron charge and J_d is dark current density. By calculation, the maximum value of D^* was 1.51×10^{11} $cmHz^{1/2}W^{-1}$ (Jones) under 365 nm illumination at low photo power density of 0.3 $mWcm^{-2}$ and bias voltage of 2 V as shown in Fig. 4(e).

To further evaluate the performance of the NiO/SiO_2/ZnO heterostructure photodetector, we measured the transient photoresponse behavior to the incident square light with a frequency of 0.1 Hz by turning on or off light source as shown in Fig. 4(f) and (h). Under 365 nm light illumination, the photodetector displayed good stability and reproducibility. To compare the response time in more detail, the rise and decay curves, which consist of a fast-response and a slow-response components, can be fitted by a biexponential relaxation equation below [30, 31]:

$$I = I_0 + Ae^{-t/\tau_1} + Be^{-t/\tau_2} \tag{3}$$

where I_0 is steady state photocurrent, t is time, A and B are two constants, and τ_1 and τ_2 are two relaxation time constants. As shown in Fig. 4(g) and (i), the rise and decay curves were well-fitted. It is worth noting that the rise time (τ_r) was relatively short having a duration of 0.048 s (Fig. 4(g)) and 0.051 s (Fig. 4(i)). The decay time (τ_d) consisting of two components, such as τ_{d1} and τ_{d2}, were estimated to be 0.108 s and 1.660 s, respectively at -0.1 V bias; 0.116 s and 1.727 s, respectively, at 0.5 V bias. Hence, the p-NiO/SiO_2/n-ZnO photodetector exhibited a fast response at low power consumption.

External quantum efficiency (EQE), which represents the ratio of the number of electrons collected to the number of incident photons, can be calculated by the equation [32]:

$$\mathrm{EQE} = \frac{hcR_\lambda}{e\lambda}$$

(4)

where h is Planck constant, c is light speed, λ is wavelength of incident light and R_λ is responsivity under specific wavelength. The photodetector exhibited remarkable EQE of 1.96×10^3 % under 365 nm illumination, which indicated a high optical gain inside the device. This optical gain could due to the inclusion of SiO_2 interlayer that suppressed surface defects at the NiO film and therefore improving the interface of p-NiO/n-ZnO heterojunction [33]. This would allow more photogenerated carriers to be collected by the electrodes across the interface, resulting in a high optical gain. Thus, the p-NiO/SiO_2/n-ZnO photodetector demonstrated excellent sensitivity in the detection of UV light. Table 1 compares the main characteristic parameters of NiO/SiO_2/ZnO photodetectors reported in this work and other UV photodetectors based on metal oxide heterostructures.

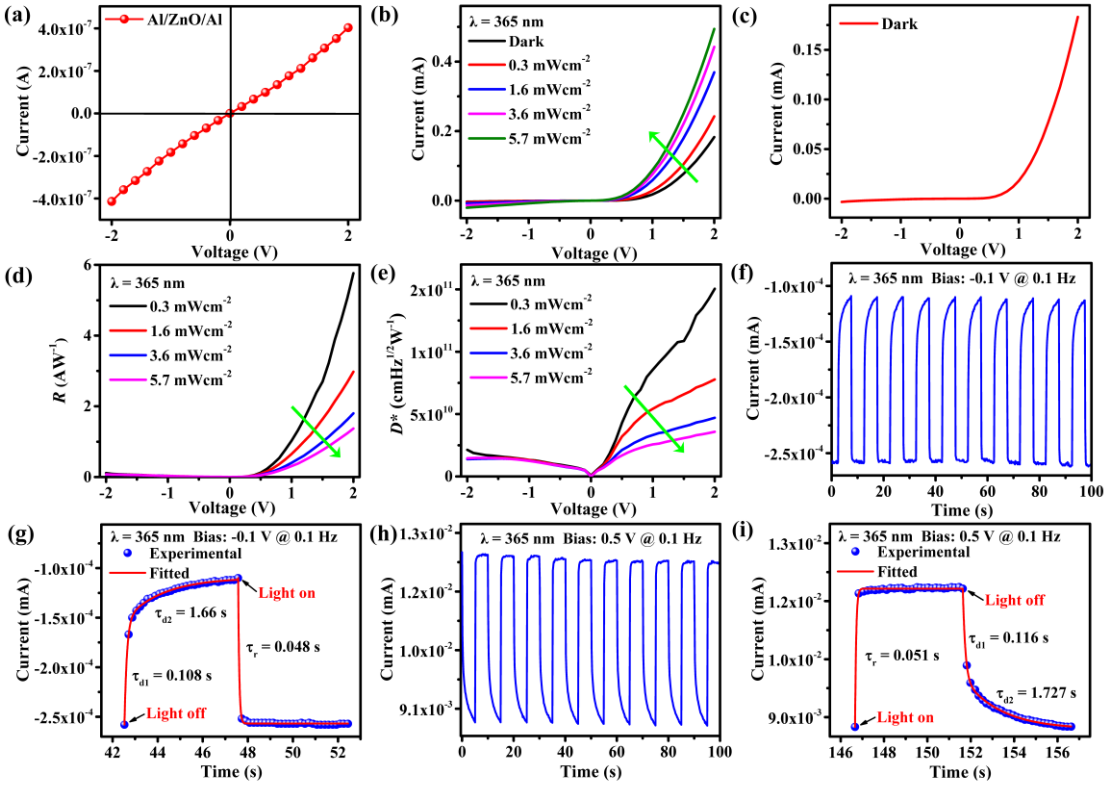

Fig. 4. (a) *I-V* plot of Al/ZnO/Al structure. (b) *I-V* curves of the NiO/SiO_2/ZnO photodetector under 365 nm light at different power densities. (c) *I-V* curve of the dark condition. (d)-(e) *R* and *D**, respectively, of the photodetector at different bias voltages under 365 nm light. (f) and (h) Illuminated by 365 nm light of the NiO/SiO_2/ZnO photodetector with an intensity of 0.6 $mWcm^{-2}$ by on/off switching at -0.1 V and 0.5 V biases. (g) and (i) Enlarged views of the rise/decay edges and exponential fitting curves corresponding to (f) and (h), respectively.

Table 1

Comparison of characteristic parameters of UV photodetectors based on metal oxide heterostructures.

Detector	Preparation method	Wavelength (nm)	R (AW^{-1})	D^* (Jones)	Ref.
$NiO/SiO_2/ZnO$	Magnetron sputtering	365	5.77	1.51×10^{11}	This work
$NiO/SiO_2/ZnO$	Magnetron sputtering/ PECVD/Hydrothermal	365	—	—	[19]
β-Ga_2O_3/SnO_2	CVD	250	1.15	5×10^{12}	[34]
β-Ga_2O_3/ZnO	Magnetron sputtering	254	0.35	—	[35]
CuO/SnO_2	Sputtering	290	10.3	—	[36]
NiO/ZnO	Low-temperature sputtering	370	0.19	3.8×10^{12}	[37]
NiO/IGZO	Magnetron sputtering	370	0.02	—	[38]
NiO/TiO_2	Two-step anodization	365	86	2.2×10^{10}	[39]

4. Conclusions

In summary, UV photodetector based on p-NiO/SiO_2/n-ZnO heterostructures was successfully fabricated using RF magnetron sputtering method. The device demonstrated good rectification characteristics (e.g., I_{dark}(+2 V)/I_{dark}(-2 V) ~ 57), low reverse saturation dark current of 3.2 μA, good stability and fast response with rise time of 0.048 s at a low power consumption of -0.1 V bias. It also exhibited a remarkably high R of 5.77 AW^{-1} under 365 nm illumination at photo power density of 0.3 $mWcm^{-2}$ with device biased at 2 V. The maximum D^* and EQE were 1.51×10^{11} Jones and 1.96×10^3 %, respectively. Importantly, the photodetector demonstrated excellent performance while consuming low power.

Acknowledgments

This work was supported by the National Natural Science Foundation of China [grant numbers 61106098, 51462037, 11864044, 61965016, 61765015, 61475026, 61275135, 61108029 and 62175209]; the Key Project of Applied Basic Research of Yunnan Province, China [grant number 2012FA003]; the Top Talents Program of Yunnan Province [grant numbers 2016HE009 and 2016HE010]; and the Scientific Research Fund project of Yunnan Education Department, China [grant number 2022Y056].

Declaration of Competing Interest

The authors declare that they have no known competing financial interests or personal relationships that could have appeared to influence the work reported in this paper.

Appendix A. Supplementary material

Supplementary data to this article can be found online at xxx.

References

[1] L. Sang, M. Liao, M. Sumiya, A comprehensive review of semiconductor ultraviolet photodetectors: from thin film to one-dimensional nanostructures, Sensors 13 (8) (2013) 10482-10518.

[2] X.G. Zheng, Q.S. Li, J.P. Zhao, D. Chen, B. Zhao, Y.J. Yang, L.C. Zhang, Photoconductive ultraviolet detectors based on ZnO films, Appl. Surf. Sci. 253 (4) (2006) 2264-2267.

[3] N. Nasiri, R.H. Bo, F. Wang, L. Fu, A. Tricoli, Ultraporous Electron-Depleted ZnO Nanoparticle Networks for Highly Sensitive Portable Visible-Blind UV Photodetectors, Adv. Mater. 27 (29) (2015) 4336-4343.

[4] X. Liu, L. Gu, Q. Zhang, J. Wu, Y. Long, Z. Fan, All-printable band-edge modulated ZnO nanowire photodetectors with ultra-high detectivity, Nat. Commun. 5 (2014) 4007.

[5] M. Tyagi, M. Tomar, V. Gupta, P-N Junction of NiO Thin Film for Photonic Devices, IEEE Electron Device Lett. 34 (1) (2013) 81-83.

[6] M. Patel, H.-S. Kim, J. Kim, All Transparent Metal Oxide Ultraviolet Photodetector, Adv. Electron. Mater. 1 (11) (2015) 1500232.

[7] G. Liu, M. Zhang, D. Zhang, X. Gu, F. Meng, S. Wen, Y. Chen, S. Ruan, Effects of growth substrates on the morphologies of TiO_2 nanowire arrays and the performance of assembled UV detectors, Appl. Surf. Sci. 315 (2014) 55-58.

[8] D.-Y. Zhang, C.-W. Ge, J.-Z. Wang, T.-F. Zhang, Y.-C. Wu, F.-X. Liang, Single-layer graphene-TiO_2 nanotubes array heterojunction for ultraviolet photodetector application, Appl. Surf. Sci. 387 (2016) 1162-1168.

[9] H. Chen, L. Hu, X. Fang, L. Wu, General Fabrication of Monolayer SnO_2 Nanonets for High-Performance Ultraviolet Photodetectors, Adv. Funct. Mater. 22 (6) (2012) 1229-1235.

[10] W. Tian, T. Zhai, C. Zhang, S.L. Li, X. Wang, F. Liu, D. Liu, X. Cai, K. Tsukagoshi, D. Golberg, Y. Bando, Low-cost fully transparent ultraviolet photodetectors based on electrospun ZnO-SnO_2 heterojunction nanofibers, Adv. Mater. 25 (33) (2013) 4625-4630.

[11] D. Guo, Y. Su, H. Shi, P. Li, N. Zhao, J. Ye, S. Wang, A. Liu, Z. Chen, C. Li, W. Tang, Self-Powered Ultraviolet Photodetector with Superhigh Photoresponsivity (3.05 A/W) Based on the GaN/Sn:Ga_2O_3 pn Junction, ACS Nano 12 (12) (2018) 12827-12835.

[12] Y. Li, T. Tokizono, M. Liao, M. Zhong, Y. Koide, I. Yamada, J.-J. Delaunay, Efficient Assembly of Bridged β-Ga_2O_3 Nanowires for Solar-Blind Photodetection, Adv. Funct. Mater. 20 (22) (2010) 3972-3978.

[13] S.J. Pearton, J. Yang, P.H. Cary, F. Ren, J. Kim, M.J. Tadjer, M.A. Mastro, A review of Ga_2O_3materials, processing, and devices, Appl. Phys. Rev. 5 (1) (2018) 011301.

[14] X. Wang, W. Tian, M. Liao, Y. Bando, D. Golberg, Recent advances in solution-processed inorganic nanofilm photodetectors, Chem. Soc. Rev. 43 (5) (2014) 1400-1422.

[15] M. Kim, J.-H. Seo, U. Singisetti, Z. Ma, Recent advances in free-standing single crystalline wide band-gap semiconductors and their applications: GaN, SiC, ZnO, β-Ga_2O_3, and diamond, J. Mater. Chem. C 5 (33) (2017) 8338-8354.

[16] P. Zu, P. Zu, Z. K. Tang, G. K. L. Wong, M. Kawasaki, A. Ohtomo, H. Koinuma, and Y. Segawa, Ultraviolet spontaneous and stimulated emissions prom ZnO microcrystallite thin films at room temperature, Solid Slate Commun. 103 (8) (1997) 459-463.

[17] D.Y. Kim, J. Ryu, J. Manders, J. Lee, F. So, Air-Stable, Solution-Processed Oxide p-n Heterojunction Ultraviolet Photodetector, ACS Appl. Mater. Interfaces 6 (3) (2014) 1370-1374.

[18] Z.M. Zhang, Y. Ning, X.S. Fang, From nanofibers to ordered ZnO/NiO heterojunction arrays for self-powered and transparent UV photodetectors, J. Mater. Chem. C 7 (2) (2019) 223-229.

[19] Y.R. Li, C.Y. Wan, C.T. Chang, Y.C. Huang, W.L. Tsai, I.C. Lee, H.C. Cheng, Sensitivity enhancement of ultraviolet photodetectors with the structure of p-NiO/insulator-SiO_2/n-ZnO nanowires, IEEE Electron Device Lett. 36 (8) (2015) 850-852.

[20] Y.F. Zhang, T. Ji, W.L. Zhang, G.Q. Guan, Q.L. Ren, K.B. Xu, X.J. Huang, R.J. Zou, J.Q. Hu, A self-powered broadband photodetector based on an n-Si(111)/p-NiO heterojunction with high photosensitivity and enhanced external quantum efficiency, J. Mater. Chem. C 5 (47) (2017) 12520-12528.

[21] Y. Kozuka, A. Tsukazaki, M. Kawasaki, Challenges and opportunities of ZnO-related single crystalline heterostructures, Appl. Phys. Rev. 1 (1) (2014) 011303.

[22] Y. Cai, L. Tang, J. Xiang, R. Ji, S.K. Lai, S.P. Lau, J. Zhao, J. Kong, K. Zhang, High performance ultraviolet photodetectors based on ZnO nanoflakes/PVK heterojunction, Appl. Phys. Lett. 109 (7) (2016) 073103.

[23] M. Jia, F. Wang, L. Tang, J. Xiang, K.S. Teng, S.P. Lau, High-performance deep ultraviolet photodetector based on NiO/beta-Ga_2O_3 heterojunction, Nanoscale Res. Lett. 15 (1) (2020) 47.

[24] Y. Zhao, L. Tang, S. Yang, K. Seng Teng, S. Ping Lau, Infrared photodetector based on GeTe nanofilms with high performance, Opt. Lett. 45 (5) (2020) 1108-1111.

[25] Y. Kokubun, S. Kubo, S. Nakagomi, All-oxide p-n heterojunction diodes comprising p-type NiO and n-type β-Ga_2O_3, Appl. Phys. Express 9 (9) (2016) 091101.

[26] S.-M. Youn, M.-J. Park, J.H. Kim, C. Jeong, Performance enhancement of CIGS thin-film solar cells with a functional-window NiO thin layer, J. Alloys Compd. 836 (2020) 154803.

[27] N. Zhu, K. Ma, X. Xue, J. Su, The formation and role of the SiO_2 oxidation layer in the 4H-SiC/β-Ga_2O_3 interface, Appl. Surf. Sci. 581 (2022) 151956.

[28] Y. Zheng, X. Tang, Y. Yang, W. Wang, G. Li, Vertically aligned GaN nanorod arrays/p-Si heterojunction self-powered UV photodetector with ultrahigh photoresponsivity, Opt. Lett. 45 (17) (2020) 4843-4846.

[29] Y. Li, D. Zhang, R. Lin, Z. Zhang, W. Zheng, F. Huang, Graphene interdigital electrodes for improving sensitivity in a Ga_2O_3:Zn deep-ultraviolet photoconductive detector, ACS Appl. Mater. Interfaces 11 (1) (2019) 1013-1020.

[30] D.Y. Guo, Z.P. Wu, Y.H. An, X.C. Guo, X.L. Chu, C.L. Sun, L.H. Li, P.G. Li, W.H. Tang, Oxygen vacancy tuned Ohmic-Schottky conversion for enhanced performance in β-Ga_2O_3 solar-blind ultraviolet photodetectors, Appl. Phys. Lett. 105 (2) (2014) 023507.

[31] D. Guo, H. Liu, P. Li, Z. Wu, S. Wang, C. Cui, C. Li, W. Tang, Zero-Power-Consumption Solar-Blind Photodetector Based on beta-Ga_2O_3/NSTO Heterojunction, ACS Appl. Mater. Interfaces 9 (2) (2017) 1619-1628.

[32] X. Xu, J. Chen, S. Cai, Z. Long, Y. Zhang, L. Su, S. He, C. Tang, P. Liu, H. Peng, X. Fang, A real-time wearable UV-radiation monitor based on a high-performance p-CuZnS/n-TiO_2 photodetector, Adv. Mater. 30 (43) (2018) e1803165.

[33] Z. Chen, B. Li, X. Mo, S. Li, J. Wen, H. Lei, Z. Zhu, G. Yang, P. Gui, F. Yao, G. Fang, Self-powered narrowband p-NiO/n-ZnO nanowire ultraviolet photodetector with interface modification of Al_2O_3, Appl. Phys. Lett. 110 (12) (2017) 123504.

[34] M.-M. Fan, L. Cao, K.-L. Xu, X.-Y. Li, Mixed-phase β-Ga_2O_3 and SnO_2 metal-semiconductor-metal photodetectors with extended detection range from 293 nm to 330 nm, J. Alloys Compd. 853 (2021) 157080.

[35] D.Y. Guo, H.Z. Shi, Y.P. Qian, M. Lv, P.G. Li, Y.L. Su, Q. Liu, K. Chen, S.L. Wang, C. Cui, C.R. Li, W.H. Tang, Fabrication of β-Ga_2O_3/ZnO heterojunction for solar-blind deep ultraviolet photodetection, Semicond. Sci. Technol. 32 (3) (2017) 03LT01.

[36] T. Xie, M.R. Hasan, B. Qiu, E.S. Arinze, N.V. Nguyen, A. Motayed, S.M. Thon, R. Debnath, High-performing visible-blind photodetectors based on SnO_2/CuO nanoheterojunctions, Appl. Phys. Lett. 107 (24) (2015).

[37] M.R. Hasan, T. Xie, S.C. Barron, G. Liu, N.V. Nguyen, A. Motayed, M.V. Rao, R. Debnath, Self-powered p-NiO/n-ZnO heterojunction ultraviolet photodetectors fabricated on plastic substrates, APL Mater. 3 (10) (2015).

[38] H.K. Li, T.P. Chen, S.G. Hu, X.D. Li, Y. Liu, P.S. Lee, X.P. Wang, H.Y. Li, G.Q. Lo, Highly spectrum-selective ultraviolet photodetector based on p-NiO/n-IGZO thin film heterojunction structure, Opt. Express 23 (21) (2015) 27683-27689.

[39] S. Pansri, R. Supruangnet, H. Nakajima, S. Rattanasuporn, S. Noothongkaew, Band offset determination of p-NiO/n-TiO_2 heterojunctions for applications in high-performance UV photodetectors, J. Mater. Sci. 55 (10) (2019) 4332-4344.